CT coreflood study of transient foam flow with oil

Tang, Jinyu; Vincent-Bonnieu, Sebastien; Rossen, William R.

DOI
10.2118/196202-ms

Publication date
2019

Document Version
Final published version

Published in
Society of Petroleum Engineers - SPE Annual Technical Conference and Exhibition 2019, ATCE 2019

Society of Petroleum Engineers

SPE-196202-MS

CT Coreflood Study of Transient Foam Flow with Oil

Jinyu Tang, Delft University of Technology; Sebastien Vincent-Bonnieu, Shell Global Solutions International; William R. Rossen, Delft University of Technology

This paper was prepared for presentation at the SPE Annual Technical Conference and Exhibition held in Calgary, Alberta, Canada, 30 Sep - 2 October 2019.

Abstract

We present a CT coreflood study of foam flow with two representative oils: hexadecane C_{16} (benign to foam) and a mixture of 80 wt% C_{16} and 20 wt% oleic acid (OA) (very harmful to foam). The purpose is to understand the transient dynamics of foam, both generated in-situ and pre-generated, as a function of oil saturation and type. Foam dynamics with oil (generation and propagation) are quantified through sectional pressure-drop measurements. Dual-energy CT imaging monitors phase saturation distributions during the corefloods. With C_{16}, injection with and without pre-generation of foam exhibits similar transient behavior: strong foam moves quickly from upstream to downstream and creates an oil bank. In contrast, with 20 wt % OA, pre-generation of foam gives very different results from co-injection, suggesting that harmful oils affect foam generation and propagation differently. Without pre-generation, initial strong-foam generation is very difficult even at residual oil saturation about 0.1; the generation finally starts from the outlet (a likely result of the capillary-end effect). This strong-foam state propagates backwards against flow and very slowly. The cause of backward propagation is unclear yet. However, pre-generated foam shows two stages of propagation, both from the inlet to outlet. First, weak foam displaces most of the oil, followed by a propagation of stronger foam at lower oil saturation. Implicit-texture foam models for enhanced oil recovery cannot distinguish the different results between the two types of foam injection with very harmful oils. This is because these models do not distinguish between pre-generation and co-injection of gas and surfactant solution.

Keywords: foam, enhanced oil recovery, CT corefloods, foam-oil interaction, simulation

Introduction

Injection of gases (e.g., CO_2, steam, N_2 or hydrocarbon gases) is nowadays a mature enhanced oil recovery (EOR) technology (Van Bergen et al., 2004; Zuloaga et al., 2017; Baghernezhad et al., 2019). Nevertheless, gas injection EOR is in general subject to poor sweep efficiency (Orr, 2007). Foam in porous media possesses unique microstructure (bubbles separated by interconnected thin films) and reduces considerably gas mobility (Kovscek and Radke, 1993; Rossen, 1996). These features give foam injection into geological formations broad engineering applications, e.g. remediation of aquifers or soils (Hayes, 2001; Hirasaki et al.,

1997) and Carbon Capture, Utilization and Storage (Alcorn et al., 2018; Bui et al., 2018; Ren and Duncan, 2019). In the petroleum industry, both laboratory studies and field pilots identify foam as a promising technology in assisting gas injection EOR (Andrianov et al., 2011; Carpenter, 2018; Patil et al., 2018; Rossen, 1996). The application of foam for EOR mainly rests on the fact that the dramatic gas-mobility reduction caused by foam results in a remarkable increase in the sweep efficiency of gas injection and thus an increase in oil recovery. Key to the success of foam EOR is the effectiveness of foam for gas-mobility control, which is evaluated in terms of foam stability and strength (reflected through its apparent viscosity - the inverse of total relative mobility of phases).

Foam-oil displacement in reservoirs is a complex process in which the effectiveness of foam is subject to many physical factors, e.g. water saturation, salinity, oil (saturation and composition), pressure, temperature, surfactant type and concentration, rock properties, etc. (Rossen, 1996; Rossen, 2013). The impact of oil among these factors is prominent, since oil left behind in place after prior flooding is out of one's control and subsequent foam injection in most cases is unavoidably in contact with oils, most of which destabilize foam (Farajzadeh et al., 2012). However, the quantitative correlation between foam stability and oil-related factors (e.g. oil saturation S_o and composition) has remained a long-standing challenge, in particular in transient displacements (Farajzadeh et al., 2012). This gap in knowledge restricts our understanding to foam-oil interactions in geological formations and, more importantly, the reliable design of a foam EOR project.

Foam flow without oil at steady-state shows two regimes as a function of foam quality (i.e., gas volumetric fractional flow in foam) (Osterloh and Jante, 1992; Alvarez et al., 2001): high- and low-quality regimes. Tang et al. (2016; 2018) have quantified the effect of several model oils on foam through their effects on the two foam regimes. Their data demonstrate that the two regimes for steady-state foam flow without oil also apply to foam with oil, with the high-quality regime more sensitive to oil. In addition, they find in their data-fitting that the two foam regimes with oil can be captured by a widely used implicit-texture foam model in STARS simulator (Computer Modeling Group, 2015). These two regimes are often used as a starting point for deeper exploration of subsurface foam dynamics. In particular, the two regimes provide a basis for estimating foam model parameters in simulating foam EOR processes on the field scale (see, e.g., Boeije and Rossen, 2015; Rossen and Boeije, 2015). However, there is a knowledge gap concerning the transient dynamics of foam flow with oil and the confidence of using foam properties estimated from steady-state data to simulate dynamic behavior.

Many prior studies investigate transient foam flow with immobile oil, i.e. foam injection at residual oil saturation S_{or} (Myers and Radke, 2000; Jensen and Friedmann, 1987; Schramm and Novosad, 1990; Raterman, 1989). The S_{or} was achieved by pre-flushing an oil-saturated core with water and/or surfactant and was assumed to be unchanged by foam injection. As S_o was not measured directly in these studies, S_{or} may be lower to foam than to water or surfactant, given the highly increased pressure gradient with foam. Ignoring the change in S_{or} may thus cause misinterpretation of the correlation between foam dynamics with S_o.

Recent studies explore the transient behavior of foam flow with oil using CT scanning to monitor phase distributions during corefloods (Simjoo and Zitha, 2013; Simjoo et al., 2013). For simplicity, foam (comprising water and gas) or liquid phases were regarded as a single phase in their CT imaging. Foam stability without oil is controlled by limiting capillary pressure, which corresponds to a limiting water saturation Sw*, the water saturation below which foam collapses abruptly (Zhou and Rossen, 1995; Cheng et al., 2000). Tang et al. (2018) in their experimental study find that oil destabilizes foam by increasing Sw*. Nevertheless, specific water saturation or oil saturation or both is unknown when treating foam or liquid phase as a single phase. One loses insights on the correlation between S_o and foam stability (i.e. featured by Sw*). More recently, Janssen et al. (2019) investigate the creation of oil bank during foam injection, by measuring three-phase saturations. Model oil examined in their study is hexadecane, much less harmful to foam stability than some crude oils in reservoirs.

We present a CT coreflood study of foam displacement with two representative model: one benign to foam stability and the other very harmful to foam stability. A major purpose is to understand the transient dynamics of foam, both pre-generated and generated in situ by co-injection of surfactant solution and gas, as a function of oil (including oil type and oil saturation). We measure both transient and steady-state sectional pressure drops vs. time to infer foam properties and dynamics, e.g. strength, generation and propagation. The real-time three-phase distributions along a core are monitored using dual-energy CT scanning. We then relate quantitatively foam properties and dynamics to phase distributions (in particular, oil type and saturation). At the end, we discuss the implications of the experimental findings to the engineering applications and simulations of foam EOR.

Experimental design

Materials and apparatus

Materials. For the purpose of the study, two representative model oils are examined: hexadecane (C_{16}), of 99% purity, supplied by Sigma-Aldrich, and a mixture of 80 wt% C_{16} and 20 wt% oleic acid (OA), of a purity 99%, provided by Honeywell Fluka. Their effects on steady-state foam flow have been shown in a recent study of Tang et al. (2018): C_{16} is relatively benign to foam stability, whereas the mixture with 20 wt % OA greatly destabilizes foam. Here we use these two model oils to examine the detrimental effects of oil on transient dynamics of in-situ-generated and pre-generated foam during EOR processes.

The gas phase is pure nitrogen (N_2) with a purity of 99.98%. The foaming agent is BIO-TERGE AS-40K AOS (C_{14-16} alpha-olefin-sulfonate), delivered with an activity of 40%, that is used directly as received from the provider Stepan company in USA. Surfactant solutions are prepared using deionized water from the Water Lab of TU Delft. Surfactant concentration we use is 0.5 wt% AOS in the solution with and 3 wt% sodium chloride (Merck). Below, aqueous surfactant solution is referred to as the water phase.

The core sample is Bentheimer sandstone. Table 1 lists the physical properties of the Bentheimer core sample used in our experiments. To avoid the complexity of property changes in core samples and facilitate the comparison of experimental results, we conduct all the measurements in the same core. Isopropanol of 99.9% purity (C_3H_8O, Emplura) is used to kill foam in cleaning the core.

Table 1—Physical properties of Bentheimer core used in foam flow experiments

Properties	Quantities
Length (cm)	40 ± 0.1
Diameter (cm)	4 ± 0.1
Pore volume (cm^3)	110.5
Porosity (%)	22 ± 0.1
Absolute permeability to brine (Darcy)	2.82 ± 0.1

CT coreflood apparatus. Figure 1 shows a schematic of the CT coreflood apparatus constructed for foam flow experiments with oil. As one follows the flow path starting from the left side, water and oil are each injected using a Vindum pump (VP-12K, Vindum Engineering, Inc.). The pump can work smoothly up to 12, 000 psi (827.4 bar) and delivers oscillation-free flow rates ranging from 0. 0001-29 cm^3/min. Two pistons in the pump allow continuous injection of water or oil as needed rates. Gas is provided by a 200-bar N_2 cylinder, and its injection is controlled through a Bronkhorst gas mass-flow controller (F-111B), with a rate ranging from 0.16-160 cm^3/min (at standard pressure P and temperature T conditions). The fluids are then injected into the Bentheimer core, which is within a PEEK (polyether-ether-ketone) coreholder. The core sample is sealed with a glue of ˜ 0.2 cm, to prevent the bypass of fluids from the side of the core.

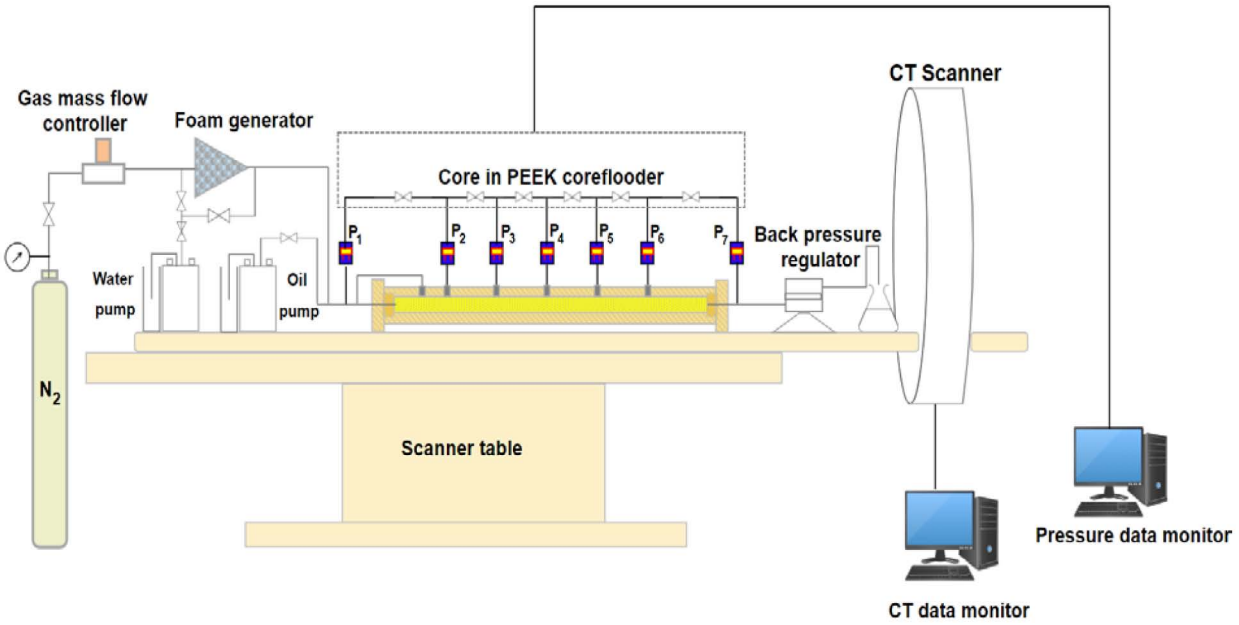

Figure 1—Schematic of CT coreflood apparatus for foam-oil flow experiments.

A back-pressure regulator is placed downstream of the coreholder to maintain P at the core outlet at 50 bar. Confining pressure, at the upstream injection pressure, is imposed by connecting the injection line to the narrow chamber between the coreholder and core sample, which is filled with water.

The whole coreflood apparatus is placed on the CT scanner table, the top portion of which is movable in both forward and backward directions. The pressure monitor records pressure drops of six sections along the core through pressure transducers (i.e. P1-7), with the first and last section of length 6.6 cm, and the four sections in the middle each of 6.7 cm. These transducers are connected to the Bentheimer core through the coreholder using PEEK tubes. The CT data monitor records CT measurements for phase distributions. The specifications of CT measurements and foam-flow experimental procedures are given in subsequent sections, with determination of phase distributions from CT images delineated in Appendix A.

CT measurements

The key parameter measured through CT scanner is the linear attenuation coefficient, $_{TCT}$ given by

$$I_{CT} = I_{CT,0}\left(\exp^{-\mu_{CT}x}\right), \tag{1}$$

where $I_{CT,0}$ is the original intensity of photons in X-ray source, I_{CT} is the intensity of photons transmitted across a material of distance x, exp denotes natural exponential, and u_{CT} is the linear attenuation coefficient. u_{CT} in the CT scanner used is linearly transformed to Hounsfield (HU) unit scale, the value of which is referred to as CT number, given as follows:

$$CT = 1000 \times \frac{\mu_{CT} - \mu_{CT,water}}{\mu_{CT,water} - \mu_{CT,air}}, \tag{2}$$

where $u_{Cr,\ water}$ and $u_{Cr,\ air}$ are respectively linear attenuation coefficients of water and air.

CT scans in this study are taken perpendicular to flow direction and start from core outlet. Each slice scanned is 2 mm in thickness, with a resolution of 512-by-512 pixels. A single scan of the whole core comprises 204 slices, with two extra slices at each end of the core, and takes in total 27 seconds. CT numbers in foam flow with oil are a function of saturations of three phases, i.e. water saturation S_w, oil saturation S_o and gas saturation S_g. To solve for S_w, S_o and S_g through measured CT numbers, one needs dual energies, each of which gives a series of independent CT numbers as a function of e.g. S_w and S_o. S_g is equal to (1 - S_w - S_o). In our CT measurements, two energy beams are used, 140 kv and 80 kv.

To distinguish water from oil, a common practice is to dope either water or oil or both to enlarge the contrast in CT number between the two phases. 140-kv and 80-kv beams are employed here and in this study. Figure 2 shows CT numbers of water doped by KI (potassium iodide) and oil doped by IDD (iododecane) in bulk, relative to cases without dopant. We find that doping oil phase alone with 20 wt% IDD gives a greater contrast between CT attenuations (HU) of water and oil than doping water or both phases: e.g., 31 HU for water vs. 1012 HU for oil with 140 kv and 56 HU for water vs. 2386 HU for oil with 80 kv (seen from Fig. 2). Specifically, the CT attenuation ratio of 140 kv / 80 kv for water (e.g., 31/56 = 0.55) is different from that for doped oil (e.g., 1012/2386 = 0.42). Therefore, the two energy beams yield two independent CT numbers (each as a function of S_w, S_o and S_g) in a single voxel. Steady-state coreflood tests by co-injecting gas, water and oil doped with 20 wt% IDD did not show noticeable difference in pressure gradient ∇P relative to that without oil dopant; this demonstrates the addition of IDD does not significantly affect foam behavior. We choose to dope oleic phase with 20 wt% IDD in our CT foam coreflood experiments.

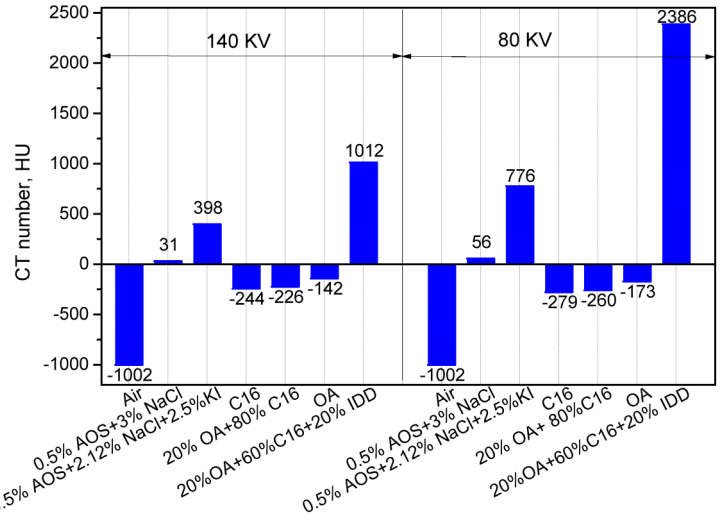

Figure 2—CT numbers of water and oil in bulk with and without dopant at a temperature of 21°C and pressure of 1 bar, in Hounsfield units (HU). IDD (iododododecane) is dopant for oil and KI (Potassium iodide), for surfactant solution. C_{16} and OA denote the model oils, hexadecane and oleic acid, and AOS is the surfactant used.

In the CT images we present below, solid red, green and blue represent 100%, 50% and 0% saturations of the given phase, respectively.

Experimental procedures

All the foam-oil flow experiments are conducted in the CT room at ~ 21°C. For three-phase saturation measurements using dual energies, one needs to follow a particular experimental sequence as follows. The specific formulas for calculating porosity and phase saturations based on measured CT numbers are described in Appendix A.

Step 1. Core sample preparation. Drill a Bentheimer core of sizes listed in Table 1. Apply a layer of glue to the radial surface of the core to prevent bypass of fluids along its side. Cut the glued core to fit the size of coreholder. Dry the core in an oven at 60°C for 48 hours. Insert the core into the coreholder and close the coreholder. Connect the coreholder to the rest of the setup and conduct gas-leakage test to ensure no leakage at elevated pressure. The following measurements are all with the back-pressure fixed at 50 bar.

Step 2. CT scan of dry core (CT_{dy}). Conduct a CT scan of the dry core before introducing any liquids.

Step 3. CT scan of wet core (CT_{wett}) and permeability test. Conduct a CT scan of a 100% brine-saturated core, and measure the absolute permeability K of the core to brine.

Step 4. CT scan of the core at connate water saturation S_{wc} to oil flood (CT_{Swc}). Flush the brine-saturated core in Step 3 with 4 PV oil until S_{wc} and take a CT scan. Our measured value of S_{wc} is comparable to SCAL (Special Core Analysis) data in Bentheimer sandstone, i.e. 0.14 - 0.18 (Andrianov et al., 2012).
Step 5. CT scan of the core at S_{orw} (waterflood residual oil saturation) (CT_{Sorw}). Flush the core at S_{wc} in step 4 with 4 PV brine until S_{orw} and take a scan. The oil saturation at 4 PV injection of brine is confirmed to be at waterflood residual oil saturation S_{orw} by 15 PV injection.
Step 6. Injection of 1 PV surfactant solution to satisfy surfactant adsorption before foam injection. Because this is not an ultralow IFT surfactant, no oil is produced during this step.
Step 7. Pressure-drop (ΔP) measurements and CT scan of the core during foam injection. Following step 6, inject foam into the core at S_{orw}, in one of two ways, i.e. either by co-injection of surfactant solution and gas or by direct injection of pre-generated foam. Upon injection, measure sectional ΔP vs. time and take CT scans according to foam responses that are reflected by the measured ΔP.
Step 8. CT scan of the core at final steady state.
Step 9. Cleaning of the core sample, following the procedures as follows:

- Kill foam from previous experiments using 4 PV isopropanol.
- Flush the core with CO_2 for 5 hours. Most isopropanol is displaced out and the rest is volatized by CO_2, to guarantee no interference of isopropanol to following foam measurements.
- Clean CO_2 with brine injection. Most CO_2 is displaced and the rest is dissolved in brine through enhancing and releasing back pressure of 50 bar several times during flush.
- Check the cleaning, by measuring core permeability K to brine. If K deviates significantly from the original value, one could repeat the steps 1 - 3 above. In our measurements, K after cleaning is within ±7% original permeability.

Step 10. Preparation of next experiment. Since the same core is used in additional experiments, steps 2 to 4 give the reference CT scans that can be applied to three-phase saturation measurements in all subsequent experiments. Thus, in each new experiment, we prepare the core and satisfy surfactant adsorption following steps 3 to 6 (without needing to take CT scans, except for step 5 to determine initial state S_{orw}), and then start foam injection and CT scans from Step 7.

Results and discussion

Table 2 gives an overview of the injection and initial conditions in each foam-oil flow experiment we conduct. In general, the experimental results we present include data on sectional ΔP along a core, saturations profiles and CT images. The data on ΔP quantify foam properties and reflect foam generation and propagation. Phase distributions obtained in CT measurements provide complementary data.

Table 2—An overview of experimental conditions in foam-oil flow experiments

Experiment	Oil type	Injection condition			Initial condition (S_{orw})	Back pressure (bar)	Remarks
		f_g	$u_t = u_g + u_w$ (ft/day)	Foam injection			
EXP-01	Hexadecane (C_{16})	91%	4.58	In-situ-generated foam	0.46± 0.02	25	Simjoo and Zitha (2013)
EXP-02		70%	4.58	Pre-generated foam	0.41± 0.02	50	
EXP-03	Mixture of	70%	4.58	In-situ-generated foam	0.39± 0.02	50	-
EXP-04	80wt% C_{16} + 20wt% OA	70%	4.58	Pre-generated foam	0.45 ± 0.02	50	-

OA denotes oleic acid, f_g (i.e., gas fractional flow in foam) is the injected foam quality.

Model oil - C_{16}

In-situ-generated foam. Studies on foam flow with less-harmful oils, e.g. C_{16}, have been reported in the literature (Simjoo and Zitha, 2013; Janssen et al., 2018). For comparison with foam flow with harmful oils, we refer to the results of Simjoo and Zitha (2013) to illustrate the transient dynamics of in-situ-generated foam flow with C_{16}.

Figure 3a, from Simjoo and Zitha (2013), shows MRF (mobility reduction factor) upon co-injection of surfactant solution and gas into a core at waterflood residual saturation of C_{16}. They define MRF as the ratio of overall pressure drop with foam to that of brine flowing at 100% water saturation. Fig. 3b is the liquid-saturation (water plus oil) profile for the case with a surfactant concentration of 0.5 wt%. The rapid increase in MRF for this surfactant concentration demonstrates that with oil benign to foam stability, strong foam could be generated immediately upon co-injection of gas and surfactant solution. Nevertheless, 2 PV of foam is injected for strong foam to propagate through the core, suggesting a delay in foam propagation. In other words, strong foam propagates with a dimensionless velocity (pore volumes occupied by strong foam divided by pore volumes of fluids injected) less than unity. We refer this phenomenon as the "retarding effect", which is caused by breaking of bubbles at the foam front. The retarding effect is also observed in many prior studies (e.g., Raterman, 1989; Bergeron et al., 1993; Mannhardt et al., 1998).

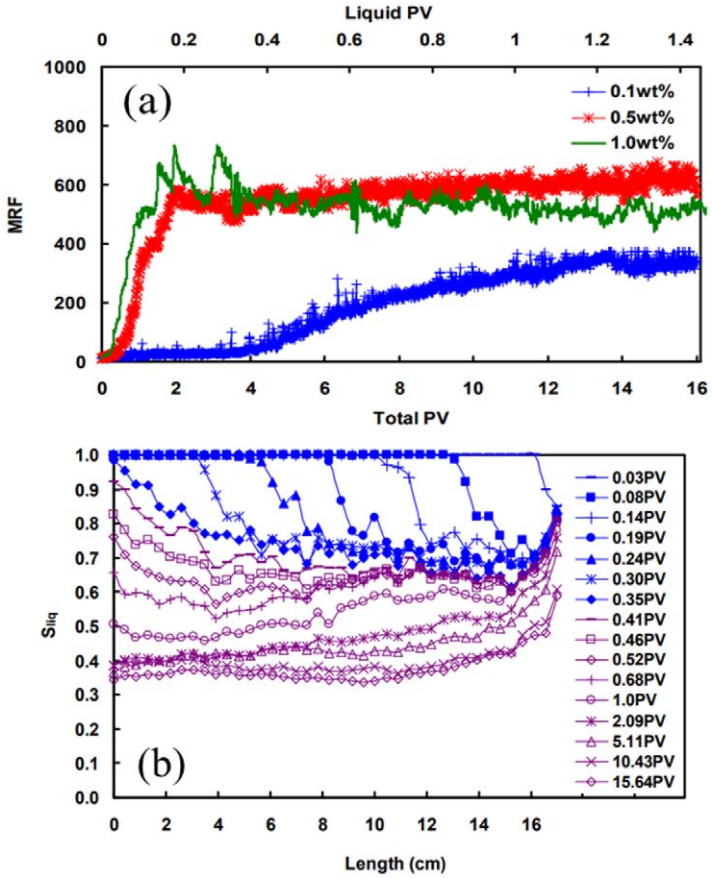

Figure 3—Data from Simjoo and Zitha (2013) on foam displacement with model oil C_{16} in a Bentheimer core initially at *SoW* (a) MRF (mobility-reduction factor); (b) liquid-saturation profile vs. position for the case with 0.5 wt% surfactant concentration. The right side corresponds to the core inlet. The injection and initial conditions are listed under EXP-01 in Table 2.

Comparing Figs. 3a and 3b shows that the increase in MRF corresponds to the forward propagation of an oil bank to the outlet within the first 2 PV injection. Strong foam propagates forward, from upstream to downstream.

Note that at steady state (e.g. 15.64 PV in Fig. 3a), liquid saturation remains greater near the inlet, thought to be an "entrance effect" in foam injection. Water and oil are plotted together in the CT images of Simjoo and Zitha. It is difficult in their data to relate MRF to oil saturation or determine if an oil bank is created by foam.

Pre-generated foam. In our own experiment in the presence of C_{16}, pre-generated foam exhibits transient behavior very similar to that with in-situ- generated foam as in Fig. 3. Figure 4 presents sectional pressure-drop (dp) history during injection of pre-generated foam into a core with C_{16} at S_{orw}. Upon injection, strong foam propagates in forward direction through the core over about 1.5 PV injection; this is comparable to the 2 PV injection (PVI) required with in-situ-generated foam in Fig. 3a. This is followed by an apparent refinement of foam texture, with sectional pressure drops at steady state increased by ~ 42%. This refinement appears to take place simultaneously throughout the core. Similar refinement is also seen in the results of Simjoo and Zitha as in Figs. 3a and 3b, after foam breakthrough at about 0.4 PV.

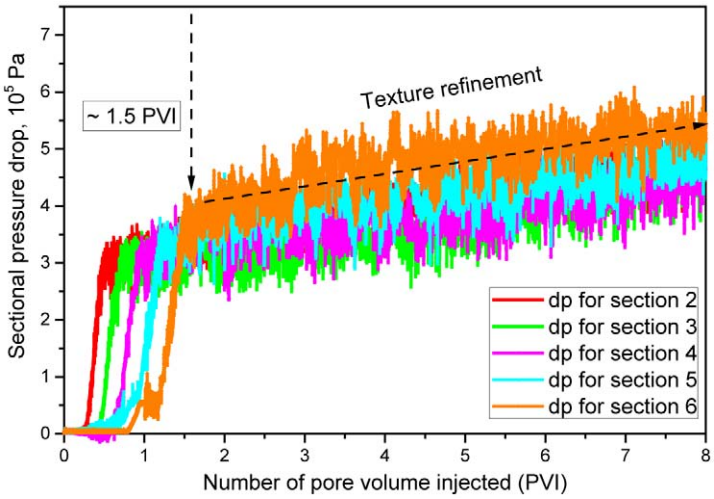

Figure 4—Sectional pressure drops vs. pore volumes injected upon injection of pre-generated foam into a Bentheimer core at S_{orw} with C_{16}. dp denotes sectional pressure drop, with sections 1 ~ 6 numbered from core inlet to outlet. The injection and initial conditions are listed under EXP-02 in Table 2.

The similar transient dynamics of foam, whether in-situ-generated or pre-generated, demonstrates that C_{16} has similar effects on foam generation and propagation. The same transient foam behavior might be expected for crude oil with components less-harmful to foam stability, such as heavy oils.

Figure 5 shows the three-phase saturation profiles as a function of dimensionless position and associated CT images (at the top) at different pore volumes injected, that correspond to the experiment in Fig. 4. Figure 5a shows that foam in the forward propagation creates an oil bank with S_o ~ 0.8 at the displacement front. Nearly 50% OOIP (Oil Originally In Place) is produced through the oil bank by the initial foam propagation, with an additional 25% OOIP produced by the refined foam, leaving 25% OOIP in place (Fig. 5c).

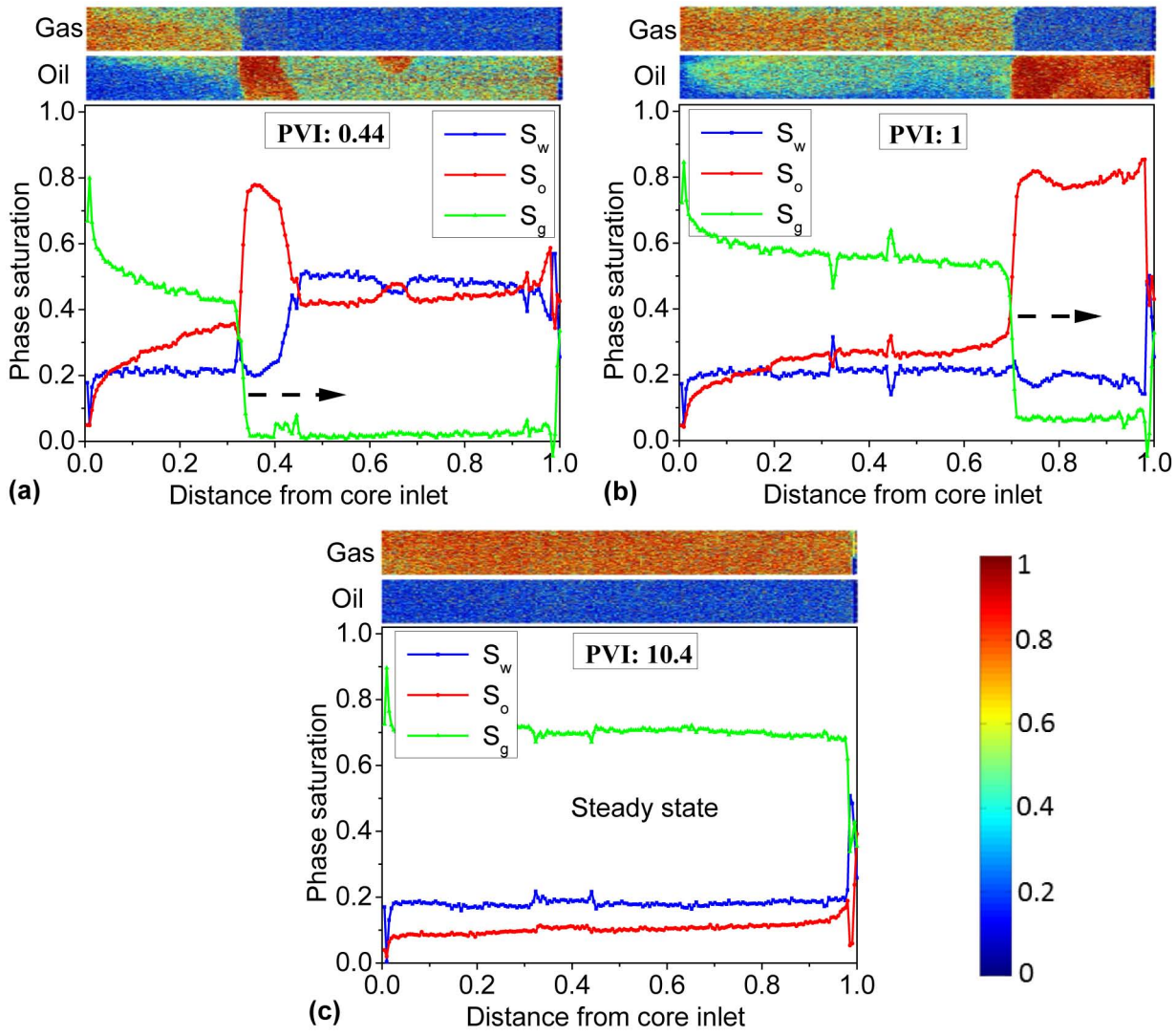

Figure 5—Phase saturation profiles vs. dimensionless position and CT scan images (on top) for gas and oil, corresponding to the foam experiment of Fig. 4 at different times: (a) 0.44 PVI; (b) 1 PVI; (c) 10.4 PVI. Foam is injected from position zero. Arrows indicate the direction of foam propagation.

S_g ~ 0 ahead of foam front seen from gas saturation profiles and CT images in Figs. 5a and 5b suggests that foam effectively prevents gas from escaping in displacing some less-harmful oils. S_g remains at ~ 0.7 at steady state (shown in Fig. 5c) including both mobilizing and trapped gas bubbles, but it is unclear of the proportion of each. The original water phase does not play a significant role in oil displacement but mainly displaced out by the oil bank rather than foam.

Model oil - mixture of 80 wt% C_{16} and 20 wt% OA. In contrast with less-harmful oils such as C_{16}, with the model oil containing 20 wt% OA, foam generated in situ upon coinjection of phases behaves very differently from pre-generated foam. The results we show below may represent transient foam behavior in reservoirs with crude oils that destabilize foam.

In-situ-generated foam

Figure 6 displays the sectional pressure-drop history upon co-injection of phases to develop in-situ foam in the Bentheimer core at S_{orw}. In this case the model oil contains 20 wt% OA; Fig. 6b on the bottom is continuation of Fig. 6a at later times. As seen from Figs. 6a and 6b, sectional pressure drops along the core do not show a significant increase except for that in the last section. Generation of strong foam begins near the core outlet. From about 25 to 40 PVI, the last sectional pressure drop keeps on rising but the others

upstream remain nearly unchanged. We ended experiment before seeing significant upstream propagation through the rest of the core (Apaydin and Kovscek, 2001; Nguyen et al., 2009).

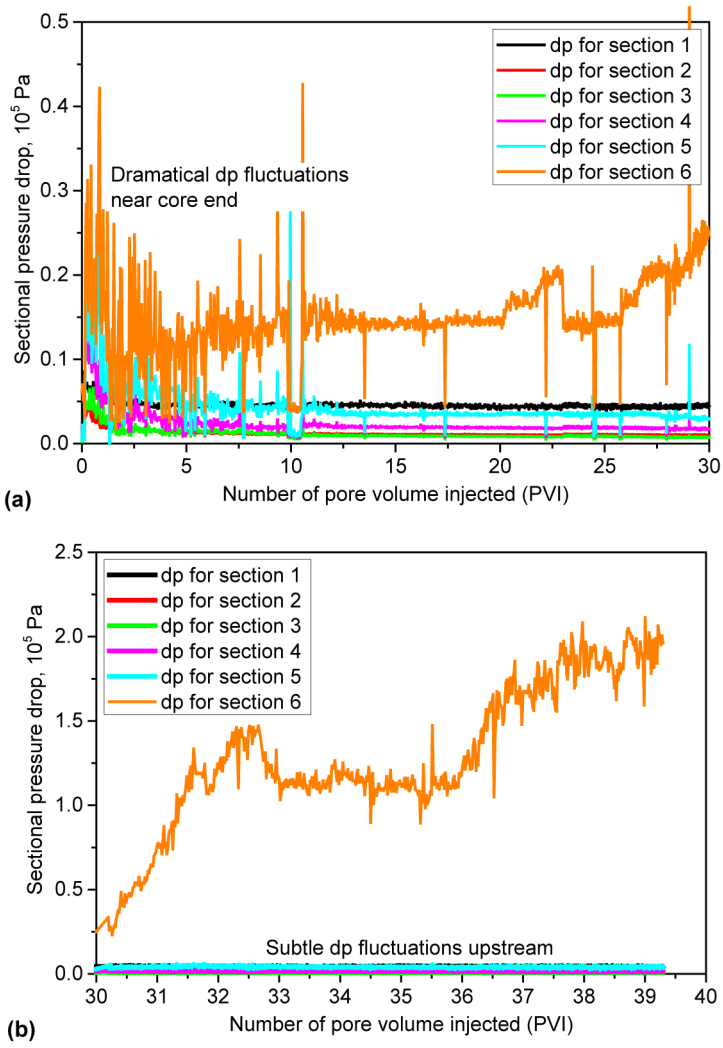

Figure 6—Sectional pressure drops vs. PVI upon co-injection of gas and surfactant solution into a Bentheimer core at Sorw, with model oil comprising 80 wt% C_{16} and 20 wt% OA: (a) 0 # 30 PVI; (b) 30 # 40 PVI. dp denotes sectional pressure drop, with sections 1 ˜ 6 numbered from core inlet to outlet. The injection and initial conditions are listed under EXP-03 in Table 2.

The initiation of strong-foam generation near the core outlet is thought to be triggered by the capillary-end effect, i.e. that capillary pressure sharply reduces to zero at the outflow face of the core (Apaydin and Kovscek, 2001). Similar behavior is reported by Shah et al. (2018), where foam is generated due to capillary effects as flow crosses a low-to-high permeability boundary. Nevertheless, capillary-end effect that occurs on a lab scale is still of uncertain relevance to the field scale.

Figure 7 gives the three-phase saturation profiles and CT images for gas and oil phases at different times for the experiment in Fig. 6. Saturation profiles in Fig. 7a suggest that prior to 0.69 PVI gas breakthrough has occurred, without displacing much oil or forming strong foam. In the second scan, taken at 33 PVI (Fig. 7b), the high gas saturation near the core outlet is consistent with the presence of strong foam there indicated in Fig. 6b. At the outflow face of the core in Fig. 7b, both water and oil saturations rise sharply whereas gas saturation drops sharply, which is an indication of capillary-end effect; this supports the preceding argument in Fig. 6 of strong-foam generation triggered by this effect.

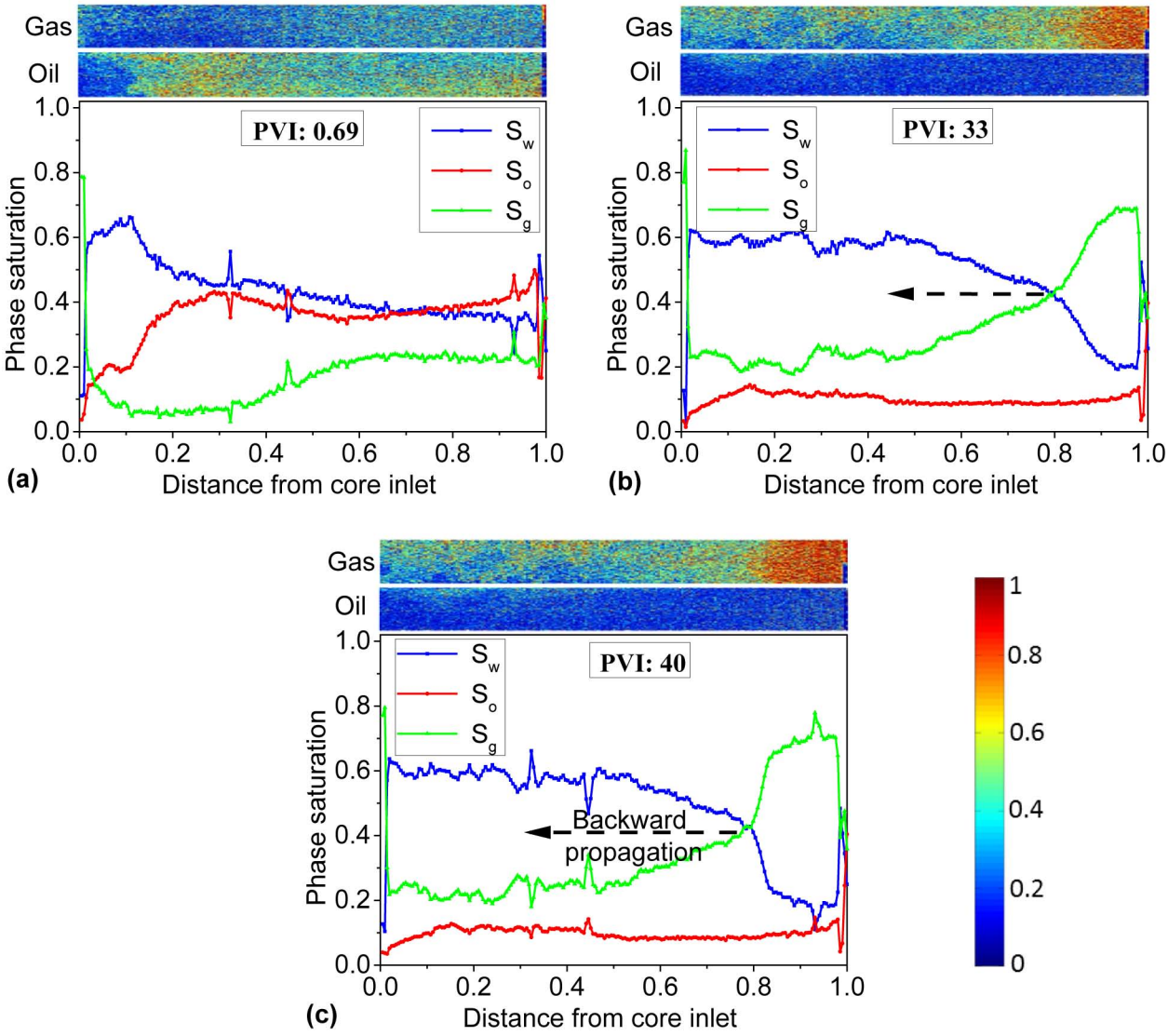

Figure 7—Phase saturation profiles vs. dimensionless position and CT scan images (on top) for gas and oil, corresponding to the foam experiment of Fig. 6 at different times: (a) 0.69 PVI; (b) 33 PVI; (c) 40 PVI. Foam is injected from position zero. Arrows mark the direction of foam propagation.

The gas and water saturation profiles near dimensionless position 0.8 in Figs. 7b and 7c suggest very slow backward propagation of strong foam. The backward propagation is also reported in the study of Apaydin and Kovscek (2001) and of Nguyen et al. (2009). From its propagation distance over 7 PVI between Figs. 7b and 7c, the foam front propagates with a dimensionless velocity roughly 0.0014. Thus, about 560 PVI would be needed for foam to propagate upstream through the core. With 33 PVI (in Fig. 7b), residual oil saturation is relatively uniform along the core and about 0.1, but foam generation still does not occur except at the core outlet. Very detrimental oils even with small quantities can significantly restrain initial foam generation.

Pre-generated foam

Figure 8 presents the sectional pressure-drop history upon direct injection of pre-generated foam into a Bentheimer core at S_{orw} with 20 wt% OA in the model oil. The evolution of sectional pressure drops suggests two stages of foam propagation: primary and secondary propagation. These two stages of propagation both start from the core inlet and march towards to the core outlet, as implied by the sequential increase in the sectional pressure drops from sections 2 - 6. Foam strength in sections 2 to 6 at 7.3 PVI in the secondary propagation increases respectively by a factor 5.2, 7, 8.35, 9.8 and 15.17 in the various sections, relative to the strength at 2.6 PVI during primary propagation.

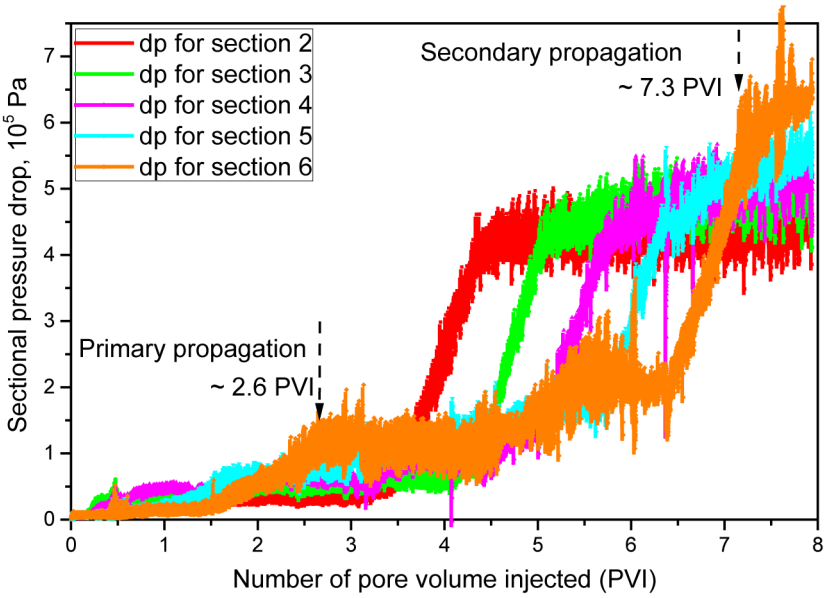

Figure 8—Sectional pressure drops vs. PVI upon injection of pre-generated foam into a Bentheimer core at *Sow*, with model oil comprising 80 wt% C_{16} and 20 wt% OA. dp denotes sectional pressure drop, with sections 1 ˜ 6 numbered from core inlet to outlet. The injection and initial conditions are listed under EXP-04 in Table 2.

Primary propagation through section 6 takes 2.6 PVI, as seen in Fig. 8. The pressure drop for the first section was not recorded due to a limitation of the apparatus, so it is difficult to determine the exact starting time of the secondary propagation. It requires more than 3.3 PVI in total after it enters section 2. It is still unclear concerning the cause for the secondary propagation (with stronger foam) being slower than the primary propagation.

Figure 9 shows the associated phase-saturation profiles and CT images for gas and oil at different times for the experiment of Fig. 8. The measured saturations and CT images in Figs. 9a and 9b show that most oil (˜ 74% OOIP) is displaced by the primary weak foam, followed by the secondary strong foam that displaces a small quantity of oil (˜ 3.8% OOIP). Gas distribution appears to be heterogeneous through the first 1.57 PVI, as seen from the gas CT images. Figure 9b suggests the secondary propagation has started before the primary propagation reaches the core outlet. Upon injection, an ultimate residual oil saturation of about 0.1 (i.e. 22.2% OOIP) remains in place (Fig. 9c).

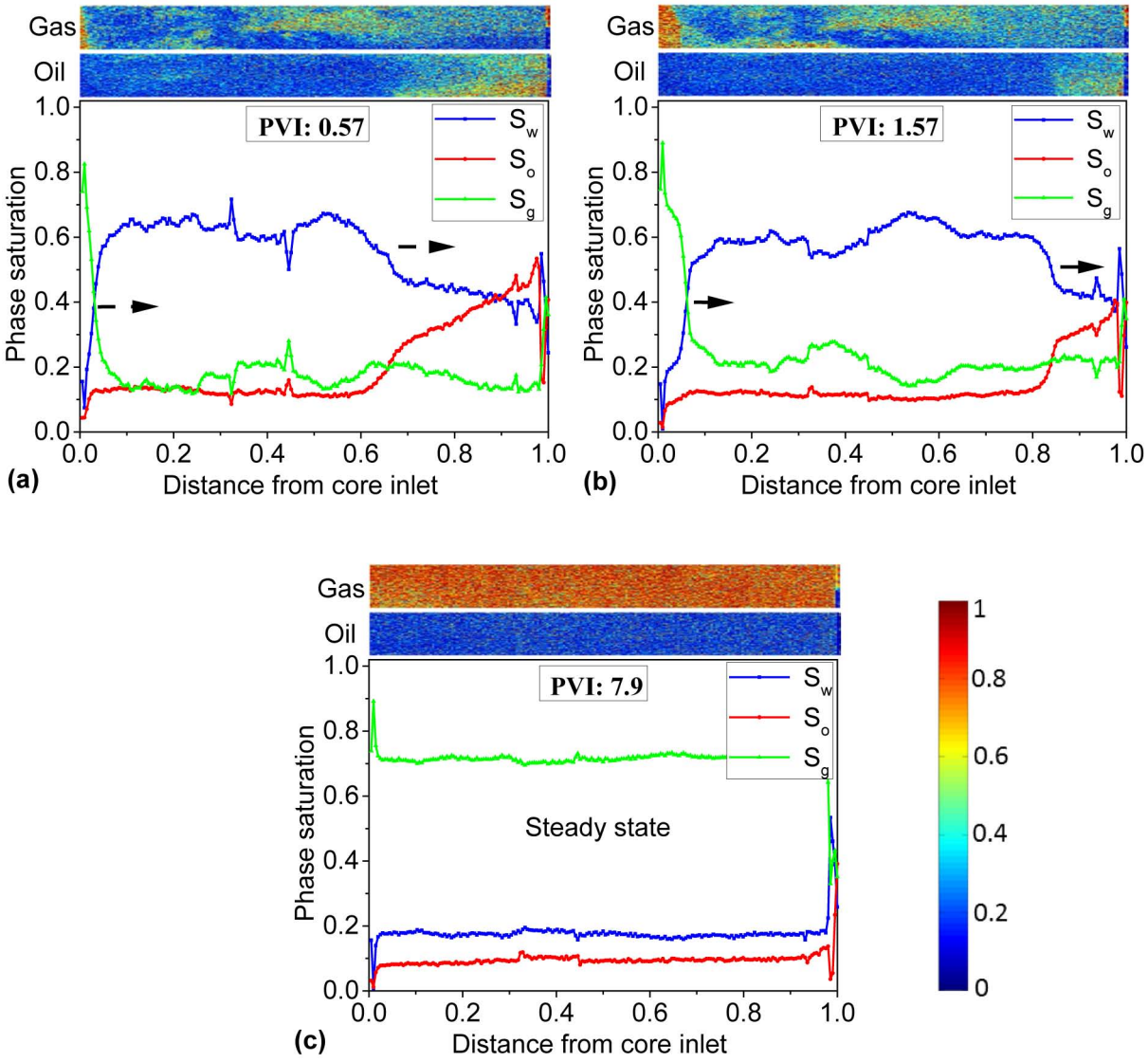

Figure 9—Phase saturation profiles vs. dimensionless position and CT scan images (on top) for gas and oil, corresponding to the foam experiment of Fig. 8: (a) 0.57 PVI; (b) 1.57 PVI; (c) 7.9 PVI. Foam is injected from position zero. Arrows indicate the foam propagation direction.

In the region between the primary and secondary propagation fronts shown in Fig. 9b, although water saturation is relatively high, no strong foam is observed. Evidently, as suggested in Figs. 6 and 7, the presence of detrimental oils even at residual oil saturation about 0.1 inhibits the generation of stronger foam. This suggests that in the presence of harmful crude oils, foam generation in absence of oil, either in the near-well region or in the wellbore, may be needed to ensure the long-distance foam propagation in reservoirs; generating foam in the presence of residual oil may be very difficult.

Implications for foam EOR and modeling.

Implications for applications of foam EOR

Statistic reported by Manrique et al. (2010) indicate that 377 out of 1507 worldwide EOR projects implement gas injection. In principle, those EOR projects that utilize gas injection are also applicable for foam injection, through which the sweep efficiency can be significantly enhanced and so does oil recovery. To ensure successful engineering applications of foam EOR, one must take into account the foam-oil interactions, in particular the stability of foam with oil in targeted reservoirs.

The experimental investigation we present provides crucial insights on two major aspects concerned with foam EOR: selection of candidate oil reservoirs and project design. Rock and fluid properties originally in an oil reservoir are out of one's control. Oils in different reservoirs have different components and thus different destabilizing effects to foam stability (Farajzadeh et al., 2012). Foam EOR works more suitably for reservoirs with less-harmful oils, e.g. unconventional heavy oils (Bagheri, 2017). To mitigate the poor injectivity of pre-generated foam, co-injection of surfactant solution and gas or SAG (surfactant-alternating-gas) may successfully make in-situ foam (Gong et al., 2019) in presence of less-harmful oils and displace it efficiently.

For those reservoirs with oils greatly detrimental to foam stability, co-injection of phases or SAG may have risks of failing in foam generation in situ, that would lead to failure of foam EOR. The injection of foam pre-formed on surface may give a good performance in improving oil production, but raise concerns about injectivity. In these situations, to develop in-situ foam with either co-injection of phases or SAG to displace oil, one needs to find surfactants or combinations of surfactants to enhance the tolerance of foam to oil. Experimental studies demonstrate that permeability contrast from low to high can assist in foam generation in the absence of oil (Falls et al., 1988; Tanzil et al., 2000; Shah et al., 2018). If it is demonstrated to work in the presence of oil, another option could be to choose those oil reservoirs with large heterogeneity to apply foam EOR.

All of our experiments are conducted in water-wet conditions. A number of recent foam EOR field pilots are carried out in carbonate reservoirs (Alcorn et al., 2018; Carpenter, 2018), which are usually oil wet. Sanchez and Hazlett concludes (1992) that foam cannot be generated in oil-wet formations with oil present, and that foam can be generated in oil-wet conditions without oil only when the formation wettability is altered by surfactant to water-wet. More efforts are needed to confirm the generality of their conclusions and understand the transient foam behavior (generation and propagation) in oil-wet reservoirs.

Implications for modeling of foam flow with oil

Foam EOR models reported in the literature in general fall into two groups: population-balance models (Kovscek et al., 1995; Kam, 2008) and implicit-texture (IT) models (Cheng et al., 2000; Computer Modeling Group, 2015; Tang et al., 2018). Population-balance models are at early stage of development in incorporating the effect of oil on foam (Myers & Radke, 2000; Ma et al., 2018). Most numerical simulations of foam EOR processes are conducted with implicit-texture models.

A widely used IT foam model, representative of current IT models, is the one in STARS simulator (Computer Modeling Group, 2015). Foam in the IT model modifies gas mobility through using a mobility reduction factor *FM to* reduce gas relative permeability (Tang et al., 2018), as follows:

$$k_{rg}^{f} = k_{rg}^{nf} \cdot FM, \tag{3}$$

$$FM = FM(S_w, S_o), \tag{4}$$

where krgf and krgnf, represent gas relative permeability with and without foam, respectively, and *FM* is a function of only saturations S_w and S_o. The representation of foam in Eqs. 3 and 4 is based on the "local-equilibrium (LE)" assumption where foam properties characterized by the factor *FM* reach immediately its final state that corresponds to given (S_w, S_o).

Current simulations assume the LE assumption applies for all cases regardless of oil type and the way of foam injection, and use directly foam-simulation parameters estimated from steady-state data to predict dynamic foam displacements with oil. Our experimental observations with less-harmful oils such as C_{16} and other prior studies without oil (Persoff et al., 1991; Kovscek et al., 2010) support the validity of the IT model.

However, IT foam models cannot distinguish the different results for co-injection of phases and direct injection of pregenerated foam as seen in Figs. 6 and 8. The reason is fundamental: without accounting for foam texture, the two cases would be simulated with identical injection conditions. It is possible that an IT

model could represent either the case of co-injection or pre-generation on its own, but not both with the same parameters. This issue needs further exploration.

Conclusions

Foam interaction with oil in geological formations remains a long-standing challenge in the process of foam enhanced oil recovery (EOR). We conduct a dual-energy CT coreflood study of foam flow with two representative model oils on the lab scale, where foam response and oil displacement is reflected by the sectional pressure drops and phase distributions. The results provide initial insights for deeper exploration of foam-oil displacement and interactions on field scales.

The generation and propagation of foam is subject to the destabilizing effects of oil on foam stability and depends in part on the injection strategy. With less-harmful oils, e.g. C_{16}, foam generated in situ upon co-injection of surfactant solution and gas shows transient dynamics similar to that with direct injection of pre-generated foam. This suggests that less-harmful oils have similar effects on foam generation and propagation. Analogous behavior could be expected for foam flow with heavy oils with compositions in general relatively benign to foam stability.

In contrast to less-harmful oils, very detrimental oils (e.g. with 20 wt% oleic acid in our study) impose very different effects on the conditions for foam generation and propagation, as implied by the completely different behavior between the two ways of foam injection. (1.) Foam generation in situ is very difficult with harmful oils in place, even at low oil saturation. The initial generation of strong foam starts at the core outlet (thought to be a result of the capillary end effect) and propagates upstream. (2.) Pre-generated foam shows two stages of propagation, both from core inlet to outlet. The primary propagation comprises weak foam that displaces most oil, followed by the secondary propagation of stronger foam.

Implicit-texture foam models for EOR simulation cannot distinguish the very different behavior between pre-generated and in-situ-generated foam with very harmful oils. It is possible that such a model could represent one process or the other. Further investigations are needed to understand this issue and to improve the prediction of foam EOR.

Acknowledgements

This project is funded by the Joint Industry Project (JIP) on Foam for Enhanced Oil Recovery at Delft University of Technology, and partly by China Scholarship Council (201406450034).

References

Alvarez, J. M., Rivas, H. J., & Rossen, W. R., (2001). Unified Model for Steady-State Foam Behavior at High and Low Foam Qualities. *SPE-74141-PA*. https://doi.org/10.2118/74141-PA.

Apaydin, O. G., & Kovscek, A. R., (2001). Surfactant Concentration and End Effects on Foam Flow in Porous Media. *Transport in porous media*, **43**(3), 511–536.

Andrianov, A., Farajzadeh, R., Nick, M. M., Talanana, M., & Zitha, P. L. J. (2011). Immiscible Foam for Enhancing Oil Recovery: Bulk and Porous Media Experiments. In *SPE-143578-MS*. SPE: *Society of Petroleum Engineers*. https://doi.org/10.2118/143578-MS.

Andrianov, A., Farajzadeh, R., Mahmoodi Nick, M., Talanana, M., & Zitha, P. L., (2012). Immiscible Foam for Enhancing Oil Recovery: Bulk and Porous media Experiments. *Industrial & Engineering Chemistry Research*, **51**(5), 2214–2226.

Alcorn, Z. P., Fredriksen, S. B., Sharma, M., Rognmo, A. U., Føyen, T. L., Fernø, M. A., & Graue, A., (2018). An Integrated CO_2 Foam EOR Pilot Program with Combined CCUS in an Onshore Texas Heterogeneous Carbonate Field. In SPE-190204-MS (p. 24). *SPE: Society of Petroleum Engineers*. https://doi.org/10.2118/190204-MS.

Bergeron, V.,; Fagan, M. E.,; Radke, C. J., (1993). Generalized Entering Coefficients: A Criterion for Foam Stability against Oil in Porous Media. *Langmuir*, **9**, 1704.

Boeije, C. S., and Rossen, W. R., (2015). "Fitting Foam-Simulation-Model Parameters to Data: I. Co-injection of Gas and Liquid," *SPE Reservoir Evaluation and Engineering*, **18**(2), 264–272.

Bagheri, S. R., (2017). Experimental and Simulation Study of the Steam-Foam Process. Part 2: The Effect of Oil on Foam Generation. *Energy & Fuels*, **31**(3), 2687–2696.

Bui, M., Adjiman, C. S., Bardow, A., Anthony, E. J., Boston, A., Brown, S., … Hackett, L. A., (2018). Carbon Capture and Storage (CCS): the Way Forward. *Energy & Environmental Science*, **11**(5), 1062–1176.

Baghernezhad, D., Siavashi, M., & Nakhaee, A., (2019). Optimal Scenario Design of Steam-assisted Gravity Drainage to Enhance Oil Recovery with Temperature and Rate Control. *Energy*, **166**, 610-623.

Cheng, L., Reme, A. B., Shan, D., Coombe, D. A., & Rossen, W. R., (2000). Simulating Foam Processes at High and Low Foam Qualities. In *SPE-59287-MS*. *SPE: Society of Petroleum Engineers*. https://doi.org/10.2118/59287-MS.

Computer Modeling Group (Calgary, Alberta, Canada), *STARS User's Guide*, Version 2015. *See also GEM User's Guide*.

Carpenter, C., (2018). Integrated CO_2-Foam Pilot in a Heterogeneous Carbonate Field. *SPE-0718-0072-JPT*, **70**(7), 72–74. https://doi.org/10.2118/0718-0072-JPT.

Falls, A. H., Hirasaki, G. J., Patzek, T. E.A., Gauglitz, D. A., Miller, D. D., & Ratulowski, T., (1988). Development of a Mechanistic Foam Simulator: the Population Balance and Generation by Snap-Off. *SPE reservoir engineering*, **3**(03), 884–892.

Farajzadeh, R., Andrianov, A., Krastev, R., Hirasaki, G. J., & Rossen, W. R., (2012). Foam-Oil Interaction in Porous Media: Implications for Foam Assisted Enhanced Oil Recovery. *Advances in Colloid and Interface Science*, 183–184, 1–13. https://doi.org/10.1016/j.cis.2012.07.002.

Gong, J., Vincent-Bonnieu, S., Bahrim, K., Zhafri, R., Mamat, C., Bakri, C. A. N., … Rossen, W. R., (2019). Modeling of Liquid Injectivity in Surfactant-Alternating-Gas Foam Enhanced Oil Recovery. *SPE Journal*.

Hirasaki, G., Miller, C., Szafranski, R., Lawson, J., & Akiya, N., (1997). Surfactant/Foam Process for Aquifer Remediation. Presented at the International symposium on oilfield chemistry, *Society of Petroleum Engineers*.

Hayes, T. D., (2001). Foam transport process for in-situ remediation of contaminated soils. U.S. Patent No. 6,210,955. Washington, DC: U.S. Patent and Trademark Office.

Janssen, M. T. G., Zitha, P. L. J., & Pilus, R. M., (2018). Oil Recovery by Alkaline-Surfactant-Foam ASF Flooding: Effect of Drive Foam Quality on Oil Bank Propagation. In *SPE-190235-MS* (p. 32). *SPE: Society of Petroleum Engineers*. https://doi.org/10.2118/190235-MS.

Janssen, M. T. G., Pilus, R. M., & Zitha, P. L. J., (2019). A Comparative Study of Gas Flooding and Foam-Assisted Chemical Flooding in Bentheimer Sandstones. *Transport in Porous Media*. https://doi.org/10.1007/s11242-018-01225-3.

Jensen, J. A., & Friedmann, F., (1987). Physical and Chemical Effects of an Oil Phase on the Propagation of Foam in Porous Media. In *SPE-16375-MS* (p. 14). *SPE: Society of Petroleum Engineers*. https://doi.org/10.2118/16375-MS.

Kam, S. I., (2008). Improved Mechanistic Foam Simulation with Foam Catastrophe Theory. *Colloids and Surfaces A: Physicochemical and Engineering Aspects*, **318**(1), 62–77.

Kovscek, A., & Radke, C., (1993). Fundamentals of Foam Transport in Porous Media. Lawrence Berkeley Lab., CA (United States).

Kovscek, A. R., Patzek, T. W., & Radke, C. J., (1995). A Mechanistic Population Balance Model for Transient and Steady- state Foam Flow in Boise sandstone. *Chemical Engineering Science*, **50**(23), 3783–3799. https://doi.org/10.1016/0009-2509(95)00199-F.

Kovscek, A. R., Chen, Q., & Gerritsen, M., (2010). Modeling Foam Displacement with the Local-Equilibrium Approximation: Theory and Experimental Verification. *SPE Journal*, **15**(1), 171–183.

Lake, L. W., Johns, R. T., Rossen, W. R., & Pope, G., (2014). Fundamentals of Enhanced Oil Recovery. Richard, Texas: *Society of Petroleum Engineers*.

Mannhardt, K.,; Novosad, J. J.,; Schramm, L. L., (1998). Foam/Oil Interactions at Reservoir Conditions. SPE 39681, presented at the SPE/DOE Improved Oil Recovery Symposium, Tulsa, OK.

Myers, T. J., & Radke, C. J., (2000). Transient Foam Displacement in the Presence of Residual Oil: Experiment and Simulation Using a Population-Balance Model. *Industrial & Engineering Chemistry Research*, **39**(8), 2725–2741. https://doi.org/10.1021/ie990909u.

Manrique, E. J., Thomas, C. P., Ravikiran, R., Izadi Kamouei, M., Lantz, M., Romero, J. L., & Alvarado, V., (2010). EOR: Current Status and Opportunities. In *SPE-130113-MS* (p. 21). *SPE: Society of Petroleum Engineers*. https://doi.org/10.2118/130113-MS.

Ma, K., Mateen, K., Ren, G., Luo, H., Bourdarot, G., & Morel, D., (2018). Mechanistic Modeling of Foam Flow Through Porous Media in the Presence of Oil: Review of Foam-Oil Interactions and an Improved Bubble Population-Balance Model. Presented at the SPE Annual Technical Conference and Exhibition, *Society of Petroleum Engineers*.

Nguyen, Q. P., Rossen, W. R., Zitha, P. L. J., & Currie, P. K., "Determination of Gas Trapping With Foam Using X-Ray Computed Tomography and Effluent Analysis". *Society of Petroleum Engineers*. (2009, June 1). doi:10.2118/94764-PA.

Osterloh, W. T., & Jante, M. J.Jr.,, (1992). Effects of Gas and Liquid Velocity on Steady-State Foam Flow at High Temperature. In *SPE-24179-MS*. SPE: *Society of Petroleum Engineers*. https://doi.org/10.2118/24179-MS

Orr, F. M., (2007). *Theory of gas injection processes* (Vol. **5**). Tie-Line Publications Copenhagen.

Persoff, P., Radke, C. J., Pruess, K., Benson, S. M., & Witherspoon, P. A., (1991). A Laboratory Investigation of Foam Flow in Sandstone at Elevated Pressure. *SPE-18781-PA*. https://doi.org/10.2118/18781-PA.

Patil, P. D., Knight, T., Katiyar, A., Vanderwal, P., Scherlin, J., Rozowski, P., … Nguyen, Q. P., (2018). CO_2 Foam Field Pilot Test in Sandstone Reservoir: Complete Analysis of Foam Pilot Response. In *SPE-190312-MS* (p. 14). *SPE: Society of Petroleum Engineers*. https://doi.org/10.2118/190312-MS.

Raterman, K. T., (1989). An Investigation of Oil Destabilization of Nitrogen Foams in Porous Media. In *SPE-19692-MS* (p. 11). SPE: *Society of Petroleum Engineers*. https://doi.org/10.2118/19692-MS.

Rossen, W. R., (1996). Foams in Enhanced Oil Recovery. In *Foams: Theory, Measurements, and Applications* (pp. 413–464). MaRcel Dekker. Retrieved from http://dx.doi.org/10.1002/food.19970410116.

Rossen, W. R., (2013). Numerical Challenges in Foam Simulation: A Review. In SPE-166232-MS. *SPE: Society of Petroleum Engineers*. https://doi.org/10.2118/166232-MS.

Rossen, W. R., and Boeije, C. S., (2015). "Fitting Foam-Simulation-Model Parameters to Data: II. Surfactant-Alternating-Gas Foam Applications," *SPE Reservoir Evaluation and Engineering*, **18**(2), 273–283.

Ren, B., & Duncan, I. J., (2019). Reservoir Simulation of Carbon Storage Associated with CO_2 EOR in Residual Oil Zones, San Andres formation of West Texas, Permian Basin, USA. *Energy*, **167**, 391–401.

Schramm, L. L., & Novosad, J. J., (1990). Micro-Visualization of Foam Interactions with a Crude Oil. *Colloids and Surfaces*, **46**(1), 21–43. https://doi.org/10.1016/0166-6622(90)80046-7.

Sanchez, J., & Hazlett, R., (1992). Foam Flow through an Oil-Wet Porous Medium: a Laboratory Study. *SPE Reservoir Engineering*, **7**(1), 91–97.

Simjoo, M., Dong, Y., Andrianov, A., Talanana, M., & Zitha, P., (2013). CT Scan Study of Immiscible Foam Flow in Porous Media for Enhancing Oil Recovery. *Industrial & Engineering Chemistry Research*, **52**(18), 6221–6233.

Simjoo, M., & Zitha, P. L.J., (2013). Effects of Oil on Foam Generation and Propagation in Porous Media. In SPE-165271-MS. *SPE: Society of Petroleum Engineers*. https://doi.org/10.2118/165271-MS.

Shah, S. Y., Wolf, K.-H., Pilus, R. M., & Rossen, W. R., (2018). Foam Generation by Capillary Snap-Off in Flow Across a Sharp Permeability Transition. Presented at the SPE Improved Oil Recovery Conference, *Society of Petroleum Engineers*.

Tanzil, D., Hirasaki, G. J., & Miller, C. A., (2000). Mobility of Foam in Heterogeneous Media: Flow Parallel and Perpendicular to Stratification. In SPE Annual Technical Conference and Exhibition. *Society of Petroleum Engineers*.

Tang, J., Vincent-Bonnieu, S., & Rossen, W., (2018). Experimental Investigation of the Effect of Oil on Steady-State Foam Flow in Porous Media. *SPE Journal*. https://doi.org/10.2118/194015-PA.

Tang, J., Ansari, M. N., & Rossen, W. R., (2019). Quantitative Modeling of the Effect of Oil on Foam for Enhanced Oil Recovery. *SPE Journal*. doi:10.2118/194020-PA

Van Bergen, F., Gale, J., Damen, K., & Wildenborg, A., (2004). Worldwide Selection of Early Opportunities for CO_2-Enhanced Oil Recovery and CO_2-Enhanced Coal Bed Methane Production. *Energy*, **29**(9-10), 1611–1621.

Zhou, Z., & Rossen, W. R., (1995). Applying Fractional-Flow Theory to Foam Processes at the "Limiting Capillary Pressure." *SPE Advanced Technology Series*, **5**(1), 154–162. https://doi.org/10.2118/24180-PA

Zuloaga, P., Yu, W., Miao, J., & Sepehrnoori, K., (2017). Performance Evaluation of CO_2 Huff-n-Puff and Continuous CO_2 Injection in Tight Oil Reservoirs. *Energy*, **134**, 181–192.

Appendix A

CT scan imaging of porosity and three-phase saturations using dual-energy

In our study, we implement 140 kv and 80 kv, denoted as 1 and 2 respectively in the following formulas. Porosity is measured using single-energy beam140 kv, calculated as follows:

$$\varphi = \frac{(CT_{wet})_1 - (CT_{dry})_1}{CT_w - CT_a} \tag{A1}$$

$(CT_{wet})_1$ = CT number of 100% brine saturated (wet) core at 140 kv, HU.
$(CT_{dry})_1$ = CT number of 100% air saturated (dry) core at 140 kv, HU.
CT_w = CT number of brine in bulk at 140 kv, HU.
CT_a = CT number of air in bulk at 140 kv, HU.

Initial state in each experiment we conduct is at waterflood residual oil saturation Sorw, which is determined using 140 kv by:

$$S_{orw} = \frac{(CT_{Sorw})_1 - (CT_{wet})_1}{(CT_{oil})_1 - (CT_{wet})_1}, \tag{A2}$$

where:

$(CT_{Sorw})_1$ = CT number of core at S_{orw} at 140 kv, HU.
$(CT_{oil})_1$ = CT number of 100% doped-oil saturated core at 140 kv, HU.

During foam injection with oil, CT attenuation combines the effects of water, oil, gas and rock matrix. For each voxel, the expressions for CT number can be written as follows:

$$(CT_{wog})_1 = (CT_{wet})_1 S_w + (CT_{dry})_1 S_g + (CT_{oil})_1 S_o, \tag{A3}$$

$$(CT_{wog})_2 = (CT_{wet})_2 S_w + (CT_{dry})_2 S_g + (CT_{oil})_2 S_o, \tag{A4}$$

$$S_g = 1 - S_w - S_o, \tag{A5}$$

where:

$(CT_{wog})_1$ = CT number of fluid saturated core involving three phases at 140 kv, HU.
$(CT_{wog})_2$ = CT number of fluid saturated core involving three phases at 80 kv, HU.
$(CT_{wet})_1$ = CT number of 100% brine saturated (wet) core at 140 kv, HU.
$(CT_{wet})_2$ = CT number of 100% brine saturated (wet) core at 80 kv, HU.
$(CT_{dry})_1$ = CT number of 100% gas saturated (dry) core at 140 kv, HU.
$(CT_{dry})_2$ = CT number of 100% gas saturated (dry) core at 80 kv, HU.
$(CT_{oil})_1$ = CT number of 100% doped-oil saturated core at 140 kv, HU.
$(CT_{oil})_2$ = CT number of 100% doped-oil saturated core at 80 kv, HU.

Substituting S_g in Eq. A4 into Eqs. A2 and A3, we solve for expressions for saturations S_o and S_w:

$$S_o = \frac{\left[(CT_{wog})_1 - (CT_{dry})_1\right]\left[(CT_{wet})_2 - (CT_{dry})_2\right] - \left[(CT_{wog})_2 - (CT_{dry})_2\right]\left[(CT_{wet})_1 - (CT_{dry})_1\right]}{\left[(CT_{oil})_1 - (CT_{dry})_1\right]\left[(CT_{wet})_2 - (CT_{dry})_2\right] - \left[(CT_{oil})_2 - (CT_{dry})_2\right]\left[(CT_{wet})_1 - (CT_{dry})_1\right]}, \tag{A6}$$

$$S_w = \frac{\left[(CT_{oil})_2 - (CT_{dry})_2\right]\left[(CT_{wog})_1 - (CT_{dry})_1\right] - \left[(CT_{oil})_1 - (CT_{dry})_1\right]\left[(CT_{wog})_2 - (CT_{dry})_2\right]}{\left[(CT_{oil})_2 - (CT_{dry})_2\right]\left[(CT_{wet})_1 - (CT_{dry})_1\right] - \left[(CT_{oil})_1 - (CT_{dry})_1\right]\left[(CT_{wet})_2 - (CT_{dry})_2\right]}. \tag{A7}$$

To measure CT_{oii}, one has to disconnect the core from the coreholder, completely dry it in an oven and then re-saturate the core with oil until S_o =100%. This will unavoidably change the original position of the core where reference CT scans are taken e. g., CT_{dry} and CT_{wet}. In our CT measurements, to avoid this risk, we estimate CT_{oil} using CT scan of the core at S_{wc} achieved by oil flood, as follows:

$$\left(CT_{oil}\right)_1 = \frac{\left(CT_{swc}\right)_1 - \left(CT_{wet}\right)_1}{1 - S_{wc}}, \tag{A8}$$

$$\left(CT_{oil}\right)_2 = \frac{\left(CT_{swc}\right)_2 - \left(CT_{wet}\right)_2}{1 - S_{wc}}, \tag{A9}$$

where S_{wc} obtained by material balance is 0.2 ± 0.02 and:

$(CT_{swc})_1$ = CT number of core at S_{wc} achieved by oil flood at 140 kv, HU.

$(C1_{swc})_2$ = CT number of core at S_{wc} achieved by oil flood at 80 kv, HU.

In our actual calculations of phase saturations, initial state S_{orw} is determined by replacing (CT_{oil}) in Eq. A2 with the right side of Eq. A8. Similarly, S_o and S_w in Eqs. A6 and A7 are finally calculated by replacing (CT_{oil}) and $(CT_{oil})_2$ with the right sides of Eqs. A8 and A9, respectively.